Fibers and Polymers 2016, Vol.17, No.4, 615-623
DOI 10.1007/s12221-016-5922-0

ISSN 1229-9197 (print version)
ISSN 1875-0052 (electronic version)

Polylactic Acid/Carbon Fiber Composites: Effects of Functionalized Elastomers on Mechanical Properties, Thermal Behavior, Surface Compatibility, and Electrical Characteristics

Chien-Teng Hsieh[1], Yi-Jun Pan[2], Ching-Wen Lou[3], Chien-Lin Huang[4], Zheng Ian Lin[5], Jo-Mei Liao[5], and Jia-Horng Lin[5,6,7]*

[1]*Department of Fashion Design and Merchandising, Shih Chien University Kaohsiung Campus, Kaohsiung 84550, Taiwan, R.O.C.*
[2]*Department of Materials and Textiles, Oriental Institute of Technology, New Taipei City 22061, Taiwan, R.O.C.*
[3]*Institute of Biomedical Engineering and Materials Science, Central Taiwan University of Science and Technology, Taichung 40601, Taiwan, R.O.C.*
[4]*Department of Fiber and Composite Materials, Feng Chia University, Taichung City 40724, Taiwan, R.O.C.*
[5]*Laboratory of Fiber Application and Manufacturing, Department of Fiber and Composite Materials, Feng Chia University, Taichung 40724, Taiwan, R.O.C.*
[6]*School of Chinese Medicine, China Medical University, Taichung 40402, Taiwan, R.O.C.*
[7]*Department of Fashion Design, Asia University, Taichung 41354, Taiwan, R.O.C.*
(Received December 11, 2015; Revised March 4, 2016; Accepted March 17, 2016)

Abstract: In this study, the maleic anhydride grafted styrene-ethylene-butylene-styrene block copolymer (SEBS-g-MA) is used as the compatilizer for polylactic acid (PLA)/carbon fiber (CF) composites. The effects of SEBS-g-MA on the mechanical properties, thermal behavior, interfacial compatibility, and electrical characteristics of composites are then evaluated. The mechanical property tests indicate that when the amount of compatilizer increases, the tensile properties and flexural property of the composites decrease while their impact strength increases. The SEM results show that the compatilizer can decrease the interstices between PLA and CF, and thereby augments their interfacial compatibility. The differential scanning calorimetry (DSC) results confirm that the compatilizer results in a greater crystallization temperature and a greater crystallinity of the composites. The electrical characteristic results indicate that neither PLA nor SEBS-g-MA is not interfered with the conductive network that is constructed by CF, which is exemplified by an average electromagnetic shielding effect of above -30 dB. This study confirms that SEBS-g-MA can improve interfacial compatibility and toughness, as well as attain good electrical characteristics of PLA/CF composites.

Keywords: Polylactic acid (PLA), Carbon fiber, Compatiblizer, Toughness, Interfacial compatibility

Introduction

Polylactic acid (PLA) is a renewable source and has great potential as a substitute for petroleum derivatives. Therefore, there have been a larger number of studies on PLA in recent years. PLA is composed by the direct polymerization of lactate or ring opening polymerization of lactide. PLA can be yielded from diverse renewable sources, including grains, potatoes, and sugar canes [1], and it can be then applied to packaging materials [2], fibrous fabrics, and various components. PLA is also a green form of energy that is featured by being biodegradable and environmentally friendly, as PLA can be decomposed into carbon dioxide, water, and humus without polluting the environment [3]. In addition, PLA has rigidity and ease of processing, which qualify it as a great candidate for industrial material. On the other hand, the disadvantages of PLA, in terms of brittleness, poor flexibility, low endurance, and low temperature resistance, can be improved by the manipulation of its structure and properties [4,5].

There are many published studies on the composites that are synthesized with other non-toxic materials in order to have greater mechanical properties as well as retain the biological properties of PLA. The additive materials include natural fibers, carbon material, and mineral powder, and the composites are thus rendered with different properties as a result of combining these different reinforcements [5-7]. Among these reinforcements, carbon fiber (CF) is an important applied engineering material. CF has excellent heat conduction and electrical conduction, and thus can be used as an electrically conductive material. When CF is blended with polymers, it is able to form a conductive network and provide the polymer matrix with electrical conduction. Meanwhile, CF also has a high specific strength and specific modulus, which reinforces the polymer matrices [8-15].

However, both PLA and CF have high strength, and their combination leads to an overly high rigidity that is unfavorable to certain applications. As a result, a modifier is then used during their combination in order to improve their interfacial compatibility [16,17], and thereby reaches the equilibrium between different mechanical properties and augments the overall strength. The toughness of PLA is often reinforced by using elastomers, which have been commonly examined

*Corresponding author: jhlin@fcu.edu.tw

in many studies. For example, Wu *et al*. used Olefin block copolymer (OBC) as reinforcement for PLA/OBC composites, and thereby significantly increased the impact strength of the PLA matrices. Ma *et al*. strengthened PLA by using ethylene vinyl acetate (EVA), and the results indicated that the pores are created as a result of the combination of rubber and matrices, which manifested a structure that predominated over the occurrence of the toughening mechanism. Afrifah *et al*. used ethyl acetate (EAC) as the modifier in order to augment the impact resistance of the composites. As a result of it increasing amount, EAC agglomerates and its agglomeration in turn withstand a greater impact load, which is exemplified by greater impact strength [18-20].

As the summary of the aforementioned literature sources indicates, the addition of elastomer can improve the toughness of PLA. In this study, carbon fibers that feature a high aspect ratio, high strengths, and electrical conductivity are used as reinforcing fillers for PLA. However, the combination of fillers simultaneously decreases the toughness of PLA. In order to compensate for this, functionalized elastomers (SEBS-g-MA) are used as the compatiblizing agent, as the succinic anhydride groups of SEBS can efficiently increase the compatibility between the PLA matrix and the CF fillers, while improving the toughness of PLA/CF composites. In addition, the combination of SEBS-g-MA on PLA/CF composites is examined in terms of mechanical properties, thermal behaviors, spherulite structure, interfacial compatibility, and electrical properties.

Experimental

Materials

Polylactic acid (PLA, 2003D, Nature Works LLC., US) has a melt flow rate (MFR) of 6 (210 ^{o}C, 2.16 kg, ASTM D1238). Carbon fiber (CF, HTS 40, Toho Tenax Industries, Inc., Japan) that is made with a PU-based sizing agent that has a length of 0.62 cm and a diameter of 7 μm. Maleic anhydride grafted styrene-ethylene-butylene-styrene block copolymer (SEBS-g-MA, FG1901 G) is purchased from Kraton Performance Polymers Ins., USA. Table 1 summarizes the characterizations of polymers.

Methods

0, 2, 4, 6, or 8 wt% of SEBS-g-MA are used as a compatilizer for the mixtures that are composed of CF and PLA masterbatches. CF is at a constant amount of 12 wt%, while PLA has different amounts according to the amounts of compatilizer. A single-screw extruder (SEVC-45, Re-Plast Extruder Corp. Taiwan, ROC) is used to mix CF, PLA, and SEBS-g-MA at a screw speed of 25 rpm, after which the mixtures are cooled and cut into composite masterbatches. The composite masterbatches are cooled with cool water, and then dried in an oven at 80 ^{o}C for 12 hours. Temperatures of the three sections for the single-screw extruder are 190 ^{o}C, 200 ^{o}C, and 200 ^{o}C, while the temperature of its die is 190 ^{o}C. The moisture of the masterbatches is removed, and an injection molding machine is used to form the samples. The temperatures of three barrels are 190 ^{o}C, 200 ^{o}C, and 200 ^{o}C, while the temperature of the die is 190 ^{o}C.

Table 1. Properties of polymers

Polymers	MFR (g/10 min)	Density (g/cm^3)	Grafted (%)
PLA	6	1.24	-
SEBS-g-MA	25-28	0.90	1.84

Tests

Tensile Test

An Instron 5566 (Instron, US) measures the tensile strength, tensile modulus, and elongation of the samples, as specified in ASTM D638. There are a total of 5 samples for each specification, and samples have a size of 115 mm×19 mm× 3.2 mm. The grip spacing is 33 mm and the tensile speed is 5 mm/min. The mean of different data are then used to analyze the variations in tensile strength, tensile modulus, and elongation of samples.

Flexural Test

An Instron 5566 (Instron, US) is used to measure the flexural strength and modulus of the samples, as specified in ASTM D790. There are five samples for each specification, and a sample has a size of 127 mm×12.7 mm×3.2 mm. The span length is 51.2 mm, and the descending rate of the compression tool is 1.5 mm/min. The mean of different data are then used to analyze the variations in flexural strength, and flexural modulus of samples.

Izod Impact Test

There are a total of five samples for each specification. The samples have a size of 63.5 mm×12.7 mm×3.2 mm, and a v-shaped cut with a depth of 2.5 mm. The impact strength of the samples is then measured by using an Izod impact tester (CPI, Atlas electric devices, US), as specified in ASTM D256. The mean of different data are then used to analyze the variations in the impact strength of samples.

Scanning Electron Microscopy (SEM)

The fractured samples that are collected from the impact test are affixed onto the base plate by using carbon paste, and are then treated with gold plating by using a gold sputter (E-1010, Hitachi, Japan). An SEM (S3000N, HITACHI, Japan) is used to observe the morphology and mechanical properties of the fractured samples with an operating voltage of 15 kV.

Differential Scanning Calorimeter (DSC)

This test is performed in a nitrogen atmosphere at 50 m*l*/ min. A 9-10 mg sample is used and kept airtight on an aluminum plate. The control group is a vacuum aluminum plate. Samples are then tested with DSC (Q200, TA Instruments, USA). The test process has an initial temperature of 40 ^{o}C.

The temperature is then rapidly increased to 200 °C at 10 °C/min increments, and samples are thus kept at 200 °C for 5 minutes in order to eliminate the heat history of the material. Samples are then cooled to 40 °C at 10 °C/min decrements, and the crystallinity, crystal temperature, and crystallization rate of PLA are observed in order to determine the influences of CF and SEBS-g-MA after they are incorporated with PLA matrices. Finally, samples are heated to 200 °C again at 10 °C/min increments in order to observe the molten condition of the samples.

The enthalpy of melting and enthalpy of crystallization of the samples are yielded according to the crystalline state and molten condition of the samples that are indicated in DSC results, and are then used to calculate the crystallinity of the samples. The equation is listed as follows.

$$X_c = \frac{\Delta H_m - \Delta H_c}{(1-\varphi)\times \Delta H_m^o} \times 100\% \quad (1)$$

where X_c is the crystallinity (%), ΔH_m is the enthalpy of melting of the samples that are removed with their heat history (J/g), ΔH_c is the enthalpy of crystallization (J/g), φ is the ratio of the fillers in the composites (%), and ΔH_m^o is the standard enthalpy of PLA when it has 100 % crystallinity of PLA (i.e., 93.6 J/g) [21].

Polarized Optical Microscopy (POM)

A slight amount of sample is placed on the glass slide, and then is heated, melted, and compressed at a temperature of 200 °C in order to form the membranes. The membranes are then cooled to 130 °C at 5 °C/min increments, and are kept at 130 °C for 90 minutes. A POM (BX51, Olympus, Japan) is used to observe the sphaerocrystals, which are compared to the thermal behaviors and mechanical properties. Meanwhile, the variations in the sphaerocrystals are recorded at isothermal temperatures but different times.

Electrical Conductivity

PLA/CF composites have been tested using the four-pin probe (KeithLink Technology Co., Ltd., Taiwan, R.O.C.) as specified in ASTM D4496-13. Samples are trimmed into 3×3×0.3 cm sections. Moreover, when the electrical conductivity is lower than 10^{-7} S/cm, samples will be measured for their resistivity (ρ) using a high resistance meter (RT-100, OHM-STAT, Static Solutions Inc., US). The electrical conductivity is computed using the following equation.

$$\sigma(\text{S/cm}) = 1/\rho = H/(R \times L \times W) \quad (2)$$

where R is the resistivity of the samples, H is the height of the sample, L is the length of the sample, and W is the width of the sample.

Electromagnetic Interference Shielding Effectiveness (EMI SE)

An electromagnetic shielding tester (E-Instrument Tech Ltd., Taiwan, R.O.C.), which is incorporated with a coaxial-line fixture (EM-2107A) that is equipped with an electromagnetic wave generator (Advantest R-3132), is used to measure the EMI SE of the samples, as specified in ASTM D4935-10. Samples are shown in Figure 1. The scan range is between 300 kHz and 3 GHz. EMI SE is presented in decibels (dB) and its equation is as follows.

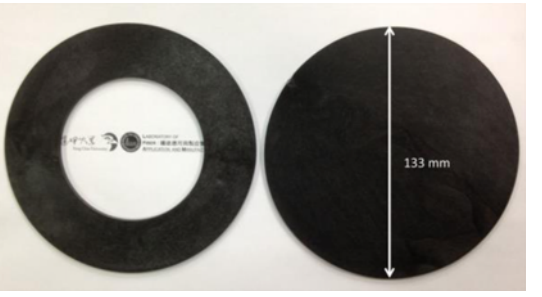

Figure 1. Image of the test samples for EMI SE measurement.

$$\text{SE} = 10\log\left[\frac{P_i}{P_o}\right] = 20\log\left[\frac{E_i}{E_o}\right] = 20\log\left[\frac{H_i}{H_o}\right] \quad (3)$$

where P_{in} is the incident energy, E_{in} is the incident electric intensity, H_{in} is the incident magnetic intensity, P_{out} is the transmitted energy, E_{out} is the transmitted electric intensity, and H_{out} is the transmitted magnetic intensity.

Results and Discussion

Mechanical Properties of PLA/CF/SEBS-g-MA Composites

Figure 2 indicates the tensile strength of PLA/CF/SEBS-g-MA composites as related to the amounts of SEBS-g-MA. In comparison to PLA/CF composites, the PLA/CF/SEBS-g-MA composites containing 8 wt% of SEBS-g-MA have a tensile strength that decreases from 110.3 MPa to 89.7 MPa. The amount of SEBS-g-MA is inversely proportional to the tensile strength of the composites. In addition, with 8 wt% of SEBS-g-MA, the tensile modulus of PLA/CF/SEBS-g-MA

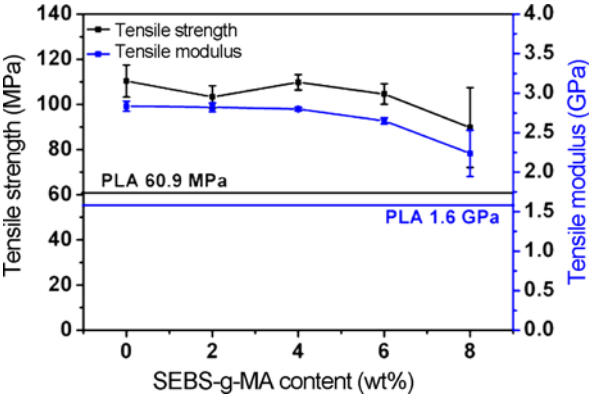

Figure 2. Tensile strength and modulus of PLA/CF/SEBS-g-MA composites, as related to various amounts of SEBS-g-MA.

composites decreases from 2835.8 MPa to 2237.3 MPa, which exemplifies the inverse relationship between the amount of compatiblizer and the tensile modulus.

The decrease in PLA/CF/SEBS-g-MA composites is primarily ascribed to the toughening effect caused by SEBS-g-MA. SEBS-g-MA is an elastomer that possesses inferior tensile properties and flexural property, and thus the tensile properties of PLA/CF/SEBS-g-MA composites decrease as a result of the increasing SEBS-g-MA. In addition, PLA has a low compatibility to CF. The succinic anhydride groups of SEBS-g-MA and the urethane groups of CF form the hydrogen bonding, thereby improving the compatibility between these two materials [22,23].

Furthermore, an externally asserted tensile stress displaces SEBS-g-MA micelle, and subsequently leaves minor pores, and thereby intrigues the micro-miniature deformation mechanism, and at the same time, provides PLA/CF/SEBS-g-MA composites with toughness. This result prevents the load from being smoothly transmitted between the matrices and fibers, and as such slightly undermines the mechanical properties of PLA/CF/SEBS-g-MA composites [24-26].

Figure 3 indicates elongation at break of PLA/CF/SEBS-g-MA composites, as related to various amounts of SEBS-g-MA. The PLA/CF/SEBS-g-MA composites have an elongation at break of 12.1 %, which is greater than that of PLA/CF composites (10.6 %). This indicates that a greater amount of SEBS-g-MA results in a greater elongation at break of the composites. PLA/CF composites are composed of PLA that has a high hardness, and CF that has a high strength, and thus the composites exhibit great strength properties. During the tensile tests, PLA/CF composites show a brittle failure when they reach their yield point after the stress is applied. This indicates their rigidity and brittleness. When SEBS-g-MA is added to the composites, the composites exhibit plastic deformation and an increasing displacement. Increasing SEBS-g-MA thus causes the yield stress and stiffness of

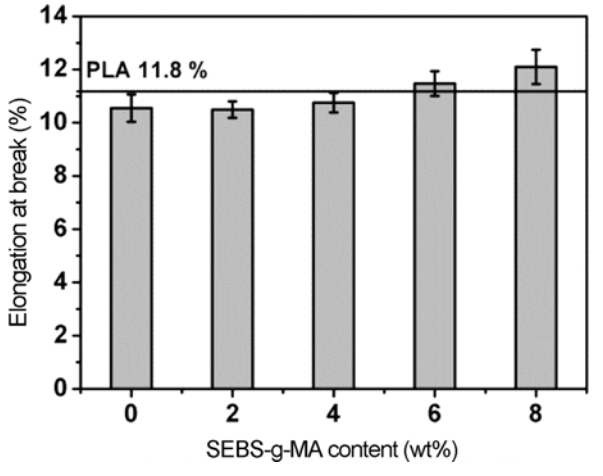

Figure 3. Elongation at break of PLA/CF/SEBS-g-MA composites, as related to various amounts of SEBS-g-MA.

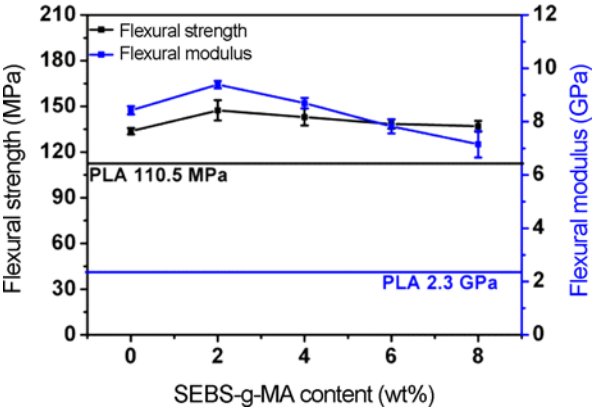

Figure 4. Flexural strength of PLA/CF/SEBS-g-MA composites, as related to various amounts of SEBS-g-MA.

PLA/CF/SEBS-g-MA to decrease. This result indicates that the equilibrium between rigidity and toughness occurs to the composites as a result of the combination of SEBS-g-MA. Due to a greater toughness of the composites, their elongation at break has an increasing trend, while their tensile strength decreases slightly [19,26].

Figure 4 indicates the flexural strength and modulus of PLA/CF/SEBS-g-MA composites as related to various amounts of SEBS-g-MA, and both the flexural strength and modulus first increase and then decrease. The flexural strength with corresponding SEBS-g-MA is 133.8 MPa (0 wt%), 147.3 MPa (2 wt%), and 136.9 MPa (8 wt%), while the flexural modulus with corresponding SEBS-g-MA is 8422 MPa (0 wt%), 9387 MPa (2 wt%), and 7132 MPa (8 wt%).

Such results are ascribed to the incorporation of SEBS-g-MA with rigid PLA/CF composites. The rigidity and the toughness of the PLA/CF/SEBS-g-MA reach equilibrium, and the shear stress and deformation mechanism allow for the composites to absorb a great amount of energy when they deform according to the damage. The greater the amount of SEBS-g-MA, the lower the flexural properties. A greater amount of SEBS-g-MA results in a greater deformation effect area, and SEBS-g-MA is an elastomer with a low strength and modulus. Therefore, the flexural properties of the composites decrease, the result of which confirms that of the study by Chow *et al*. [24].

Figure 5 indicates the impact strength of PLA/CF/SEBS-g-MA composites as related to various amounts of SEBS-g-MA. In comparison to PLA/CF composites, PLA/CF/SEBS-g-MA composites containing 8 wt% of SEBS-g-MA have a greater impact strength. The impact strength increases from 74.3 MPa to 96.0 MPa, which indicates that a greater SEBS-g-MA is conducive to the impact strength of the composites. Increases in the impact strength PLA/CF/SEBS-g-MA composites are due to the interfacial compatibility between PLA and SEBS-g-MA. Apart from chemical bonding, there

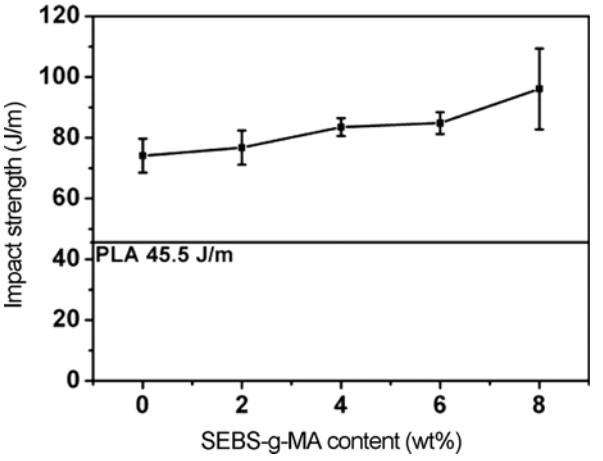

Figure 5. Impact strength of PLA/CF/SEBS-g-MA composites, as related to various amounts of SEBS-g-MA.

are also SEBS-g-MA micelles distributing in the PLA matrices, and the adhesiveness is augmented as a result of the greater contact area, the facts of which thus improves the combination of SEBS-g-MA and PLA [20]. In addition, a greater amount of SEBS-g-MA also can form a flagon region in the PLA/CF/SEBS-g-MA composites in order to absorb the impact energy, as well as contribute a dissipation factor of capacity that prevents the generation and aggravation of cracks for a greater impact strength [26].

SEM Observation of PLA/CF/SEBS-g-MA Composites

Figure 6 indicates the SEM images of PLA/CF composites and PLA/CF/SEBS-g-MA composites that are composed of various amounts of SEBS-g-MA. Increasing SEBS-g-MA reduces the interstices between PLA and CF, and causes the fiber damage vestiges that are parallel to the fractured surface. These results confirm that SEBS-g-MA enhances the interfacial compatibility between PLA and CF, which in turn augments the mechanical properties of PLA/CF/SEBS-g-MA composites. The 3K-time magnified SEM images are indicated in Figure 7, which clearly shows that cavitation occurs over the fractured surface as a result of the stripped SEBS-g-MA caused by an impact [19]. The SEBS-g-MA micelles are in a form of spherical structure. When there are greater amounts of micelles, micelles agglomerate and then deform. The micelles have a shorter distance as a result of their greater diameter, which in turn promotes the impact resistance of the composites. Such a result is approved by the results of a previous study [27]. The SEM images shown in Figures 6 and 7 indicate that an increasing amount of SEBS-g-MA results in a greater size of their micelles, which in turn exaggerates the phase separation. Figures 2-5 indicate that SEBS-g-MA content of 8 wt% results in unstable mechanical strengths of PLA/CF/SEBS-g-MA composites, exemplified by a high standard deviation. In other words, an appropriate amount of SEBS-g-MA promotes and ensures their mechanical strengths.

Thermal Behaviors of PLA/CF/SEBS-g-MA Composites

Figure 8 indicates the influence of SEBS-g-MA elastomer on the thermal behaviors of PLA/CF/SEBS-g-MA composites. The crystallization temperature of the composites increases as a result of the increasing SEBS-g-MA, while their melting temperature does not significantly fluctuate. The combination of SEBS-g-MA has a greater nucleation effect than CF. The test results indicate that the crystallization temperature of PLA/CF composites increases from 105.9 to 108.9 °C, and the crystallization temperature of PLA/CF/SEBS-g-MA composites increases from 108.9 °C to 122.3 °C with their crystallinity increasing from 3.1 % to 10.5 %, as indicated in

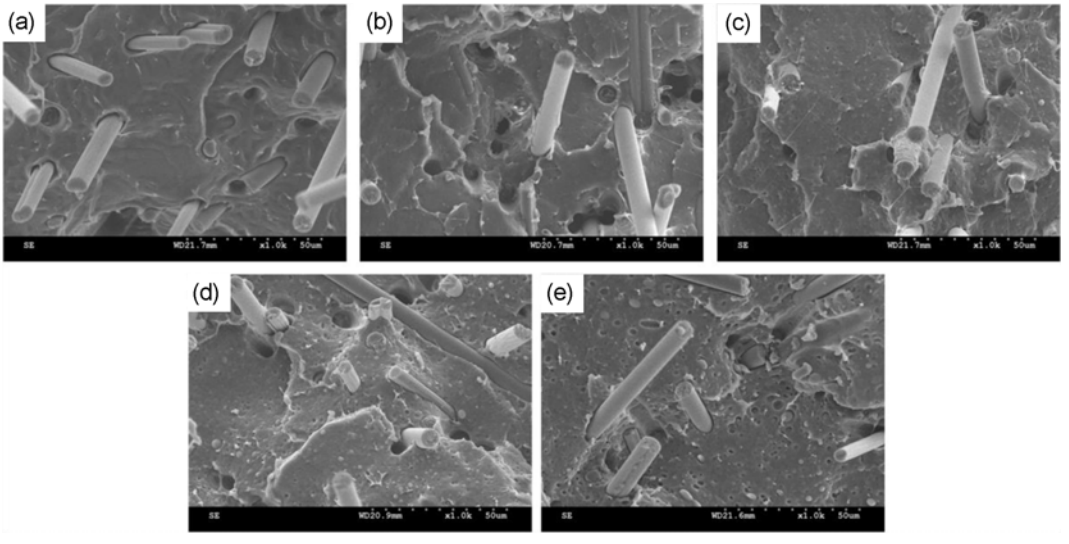

Figure 6. SEM images (1000×) of the fractured PLA/CF/SEBS-g-MA composites with a constant amount of 12 wt% of CF, and (a) 0 wt%, (b) 2 wt%, (c) 4 wt%, (d) 6 wt%, and (e) 8 wt% of SEBS-g-MA.

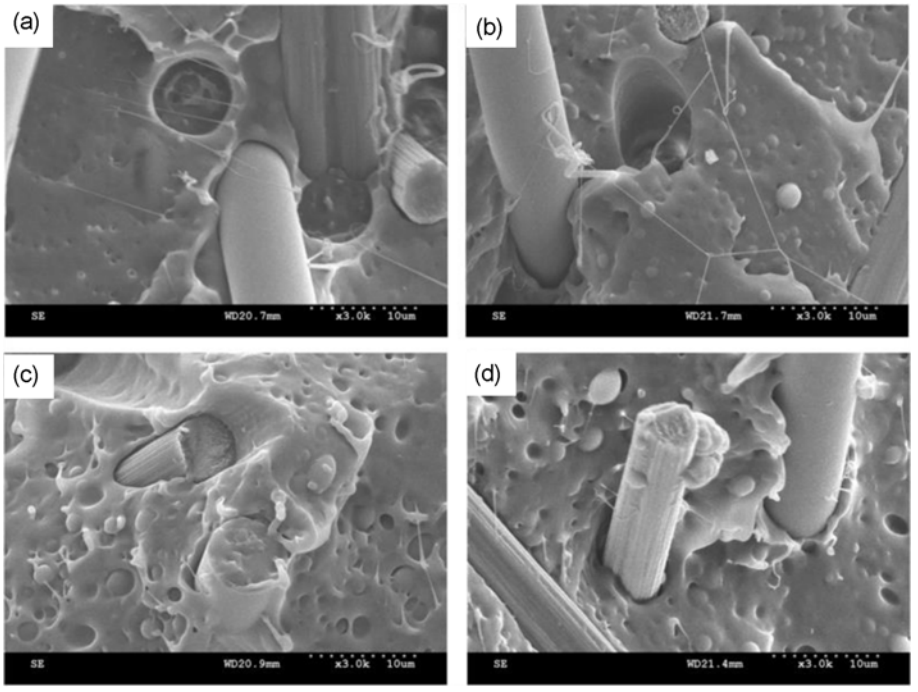

Figure 7. SEM images (3000×) of the fractured PLA/CF/SEBS-g-MA composites with a constant amount of 12 wt% of CF, and (a) 2 wt%, (b) 4 wt%, (c) 6 wt%, and (d) 8 wt% of SEBS-g-MA.

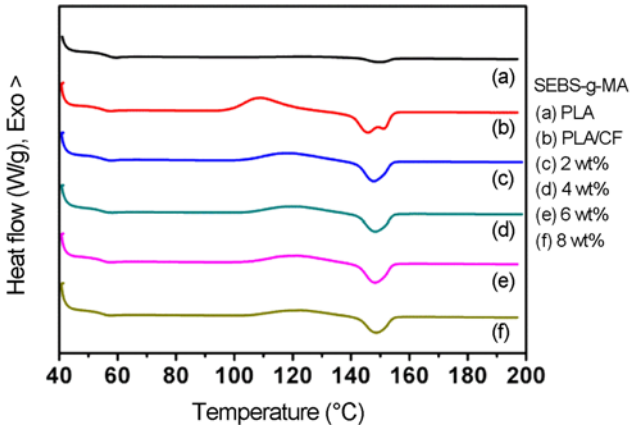

Figure 8. DSC thermal analysis of PLA/CF/SEBS-g-MA composites, as related to various amounts of SEBS-g-MA.

Table 2. This result confirms that the combination of CF can effectively increase the crystallization temperature of PLA.

In comparison with PLA/CF composites, when combined with 8 wt% of SEBS-g-MA, the crystal temperature of PLA/CF/SEBS-g-MA composites increases from 108.9 °C to 122.3 °C with their crystallinity increasing from 3.06 % to 10.45 %. A small part of SEBS-g-MA is not compatible with PLA, which results in micelles, as indicated in Figure 9. These SEBS-g-MA micelles also become nucleation agents that increase the crystallization temperature. When there is more SEBS-g-MA, there are more SEBS-g-MA micelles. As a result, a high amount of SEBS-g-MA has a positive influence on the crystallization temperature of PLA/CF/SEBS-g-MA composites. A greater amount of SEBS-g-MA also results in a greater size of SEBS-g-MA micelles, and prevents the segmental motion that is conducive to the

Table 2. Thermal properties of PLA/CF/SEBS-g-MA composites that are composed of various contents of SEBS-g-MA

SEBS-g-MA (wt%)	T_g (°C)	T_c (°C)	T_m (°C)	ΔH_m (J/g)	ΔH_c (J/g)	X_c (%)
PLA	58.8	105.9	149.1	3.6	0.8	3.1
PLA/CF	57.0	108.9	145.8	18.3	13.8	5.5
2	57.1	119.4	147.7	18.9	13.7	6.6
4	57.1	120.6	148.3	15.9	9.0	8
6	57.0	121.5	148.2	17.6	10.1	9.8
8	57.1	122.3	148.6	14.9	7.1	10.5

Note. PLA/CF composites have a specified amount of CF (12 wt%).

crystallization temperature. In contrast, the conjunction of 8 wt% of SEBS-g-MA results in a melting temperature of PLA/CF/SEBS-g-MA composites being 149 °C, which does not significantly vary by much in comparison with that of a PLA/CF composite (i.e., 145.8 °C). This result indicates that PLA/CF/SEBS-g-MA composites have high heat stabilization without being influenced by the conjunction of SEBS-g-MA [26,28].

POM Observation of PLA/CF/SEBS-g-MA Composites

The polarized optical microscopic (POM) images of pure PLA and PLA/CF/SEBS-g-MA composites that are composed of various amounts of SEBS-g-MA are indicated in Figure 9. Figure 9(a) shows the crystal growth with CF as a nucleating agent and the crystals grow at both ends of CF or where two CF intersect. As a result, there are a lower amount of sphaerocrystals that are stacked, which enables the sphaerocrystals to distribute and grow. Figure 9(b-e) shows that the increasing SEBS-g-MA results in an even distribution of crystals, as well as complete sphaerocrystal status.

Figure 9(a) indicate that when the temperature decreases to 130 °C, most sphaerocrystals start their nucleation growth along CF, and a greater crystal rate occurs and reflects that CF as a valid nucleating agent. Figure 9(c, d) shows that the SEBS-g-MA micelles have a much smaller size than that of the sphaerocrystals in PLA/CF/SEBS-g-MA composites. Simultaneously, SEBS-g-MA micelles also serve as nucleating agents, and their coalescence expedites the sphaerocrystals to distribute, followed by nucleation, growth, and eventually the yield of a complete structure. Such results confirm the results of the study by Radonjič *et al*., where a small amount of SEP elastomer formed complete sphaerocrystals with a greater size than that of pure PLA sphaerocrystals [29].

Electrical Properties of PLA/CF/SEBS-g-MA Composites

Figure 10 indicates the electrical conductivity of PLA/CF/SEBS-g-MA composites as related to various amounts of SEBS-g-MA elastomer. The electrical conductivity of the PLA/CF/SEBS-g-MA composites that contain 8 wt% of SEBS-g-MA is around 2.2×10^{-5} S/cm, which is similar to that of PLA/CF composites. Such a result states that the electrical conductivity of PLA/CF/SEBS-g-MA composites is not dependent on SEBS-g-MA, but it depends on CF that is an electrically conductive filler. In addition, the PLA/CF composites can have a complete conductive network that is constructed by the conductive filler (i.e., CF), and thus have electrical conduction [30]. On the other hand, the size of CF is relatively greater than that of SEBS-g-MA micelles, and as such, conductive CF can stride over the PLA phase and the SEBS-g-MA phase without being influenced by their

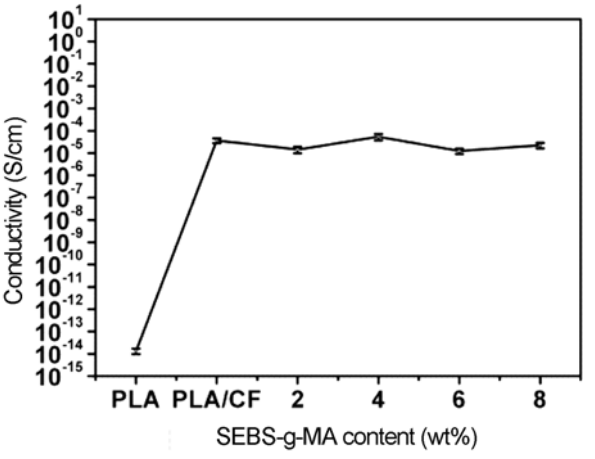

Figure 10. Electrical conductivity of PLA/CF/SEBS-g-MA composites, as related to various amounts of SEBS-g-MA.

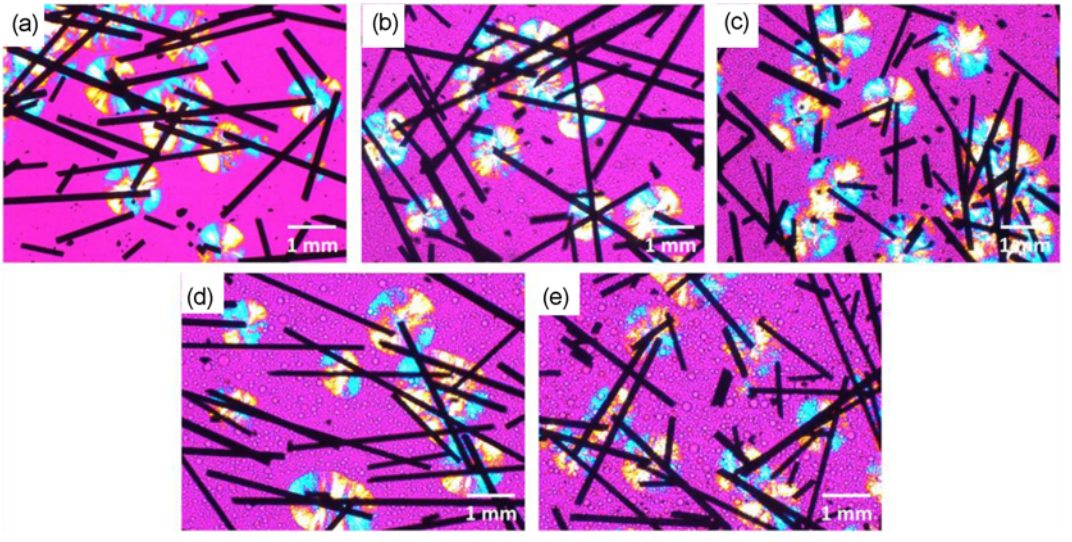

Figure 9. POM images (200×) of the fractured PLA/CF/SEBS-g-MA composites with a constant amount of 12 wt% of CF, and (a) 0 wt%, (b) 2 wt%, (c) 4 wt%, (d) 6 wt%, and (e) 8 wt% of SEBS-g-MA.

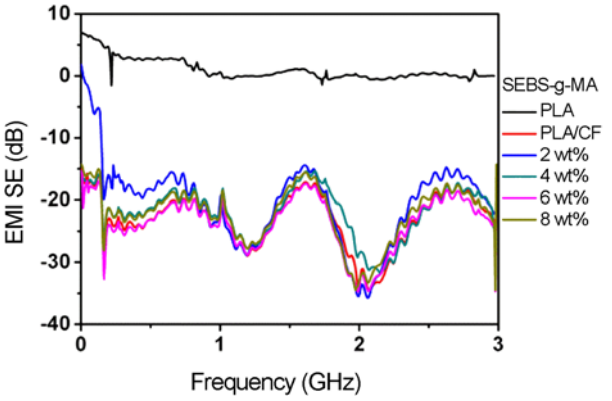

Figure 11. EMI SE of PLA/CF/SEBS-g-MA composites, as related to various amounts of SEBS-g-MA.

Table 3. EMI SE data of PLA/CF/SEBS-g-MA composites in relation to SEBS-g-MA contents

SEBS-g-MA content (%)	EMI SE (dB)		
	1 GHz	2 GHz	3 GHz
PLA	0.3	-0.5	-0.1
PLA/CF	-24.3	-34.5	-23.2
0	-23.6	-33.8	-22.1
2	-22.7	-31.2	-24.6
4	-24.6	-34.6	-23.8
8	-23.1	-33.2	-23.8

Note. PLA/CF composites have a specified amount of CF (12 wt%).

insulating properties.

Figure 11 and Table 3 indicates the EMI SE of PLA/CF/SEBS-g-MA composites, as related to various amounts of SEBS-g-MA elastomer. The EMI SE of PLA/CF composites is -34 dB, and PLA/CF/SEBS-g-MA composites have a similar EMI SE, regardless of being incorporated with various amounts of SEBS-g-MA. Namely, the EMI SE of PLA/CF/SEBS-g-MA composites does not correlate to the amounts of SEBS-g-MA. The EMI SE of the composites depends on their electrical conductivity. Materials with high conductivity are highly electrically conductive, and they can absorb the energy of electromagnetic waves and dissipate it in heat energy form. As a result, the PLA/CF/SEBS-g-MA composites have a high electrical conductivity and thus a high EMI SE [31,32]. However, PLA/CF composites have an EMI SE of beyond -30 dB, and an increase in SEBS-g-MA does not influence the EMI SE of PLA/CF/SEBS-g-MA composites. Frequencies of 1-3 GHz are commonly used as a radio spectrum in our daily lives. Table 3 indicates that the PLA/CF composites have a satisfactory EMI SE of above -20 dB in this radio spectrum, and thus reach the EMI SE grade required by livelihood commodities.

Conclusion

This study successfully reinforces the PLA/CF composites by using SEBS-g-MA as a compatilizer. The PLA/CF/SEBS-g-MA composites are then evaluated for various properties, which proved that SEBS-g-MA is a superior toughening material. When PLA/CF/SEBS-g-MA composites are incorporated with 8 wt% of SEBS-g-MA as reinforcement, their tensile strength decreases by 18.7 %, tensile modulus decreases by 26.8 %, flexural strength increases by 2.4 %, flexural modulus decreases by 18 %, and impact strength increases by 29 %. The test results have proven that SEBS-g-MA demonstrates a toughening effect over the composites, as exemplified by its significant improvement in the brittleness of PLA. According to the fractured structure of PLA/CF/SEBS-g-MA composites, SEBS-g-MA forms micelles with toughening efficacy. SEBS-g-MA micelles were distributed in PLA matrices, and thereby improve the compatibility between CF and PLA matrices in order to augment the toughness of the composites. POM observation and DSC thermal analysis also provide corresponding results. Increasing SEBS-g-MA results in a greater crystallization temperature and crystallinity. However, the conjunction of SEBS-g-MA does not undermine, and retains the electrical properties of the composites. The electrical conductivity and EMI SE of PLA/CF/SEBS-g-MA composites are 2.2×10^{-5} S/cm and -30 dB, respectively. This study successfully creates PLA/CF/SEBS-g-MA composites that have high strength, high electrical properties, and good thermal behaviors. Such composites are composed of eco-friendly PLA matrices, which can be improved and optimized by adjusting the process parameters, in order to meet different requirements. In the future, the composites are expected to be commonly applied to different packaging materials or encapsulation of outer shells.

Acknowledgements

The authors would like to thank Ministry of Science and Technology of Taiwan, for financially supporting this research under Contract MOST 104-2221-E-035-092.

References

1. R. T. Bachmann, A. C. Johnson, and R. G. J. Edyvean, *Int. Biodeter. Biodegr.*, **86**, 225 (2014).
2. I. Armentano, N. Bitinis, E. Fortunati, S. Mattioli, N. Rescignano, R. Verdejo, M. A. Lopez-Manchado, and J. M. Kenny, *Prog. Polym. Sci.*, **38**, 1720 (2013).
3. R. Auras, B. Harte, and S. Selke, *Macromol. Biosci.*, **4**, 835 (2004).
4. K. Madhavan Nampoothiri, N. R. Nair, and R. P. John, *Bioresour. Technol.*, **101**, 8493 (2010).
5. J.-M. Raquez, Y. Habibi, M. Murariu, and P. Dubois, *Prog.*

Polym. Sci., **38**, 1504 (2013).
6. A. K. Bledzki, A. Jaszkiewicz, and D. Scherzer, *Compos. Pt. A-Appl. Sci. Manuf.*, **40**, 404 (2009).
7. Y. F. Buys, T. Aoyama, S. Akasaka, S. Asai, and M. Sumita, *Compos. Sci. Technol.*, **70**, 200 (2010).
8. Z. Xu, L. Chen, Y. Huang, J. Li, X. Wu, X. Li, and Y. Jiao, *Eur. Polym. J.*, **44**, 494 (2008).
9. N. G. Karsli and A. Aytac, *Mater. Des.*, **32**, 4069 (2011).
10. Z. Dai, F. Shi, B. Zhang, M. Li, and Z. Zhang, *Appl. Surf. Sci.*, **257**, 6980 (2011).
11. M. Gashti, R. Hajiraissi, and M. Gashti, *Fiber. Polym.*, **14**, 1324 (2013).
12. T.-T. Li, R. Wang, C.-W. Lou, J.-Y. Lin, and J.-H. Lin, *Fiber. Polym.*, **15**, 315 (2014).
13. G. Salimbeygi, K. Nasouri, and A. Shoushtari, *Fiber. Polym.*, **15**, 583 (2014).
14. Z. Zhang, F. Zhang, X. Jiang, Y. Liu, Z. Guo, and J. Leng, *Fiber. Polym.*, **15**, 2290 (2014).
15. L. Zou, C. Lan, X. Li, S. Zhang, Y. Qiu, and Y. Ma, *Fiber. Polym.*, **16**, 2158 (2015).
16. J. Yang, J. Xiao, J. Zeng, L. Bian, C. Peng, and F. Yang, *Fiber. Polym.*, **14**, 759 (2013).
17. D. Jiang, L. Liu, F. Zhao, Q. Zhang, S. Sun, J. He, B. Jiang, and Y. Huang, *Fiber. Polym.*, **15**, 566 (2014).
18. M. Wu, Z. Wu, K. Wang, Q. Zhang, and Q. Fu, *Polymer*, **55**, 6409 (2014).
19. P. Ma, D. G. Hristova-Bogaerds, J. G. P. Goossens, A. B. Spoelstra, Y. Zhang, and P. J. Lemstra, *Eur. Polym. J.*, **48**, 146 (2012).
20. K. A. Afrifah and L. M. Matuana, *Macromol. Mater. Eng.*, **295**, 802 (2010).
21. H. Wang, X. Sun, and P. Seib, *J. Appl. Polym. Sci.*, **82**, 1761 (2001).
22. E. Oliaei, B. Kaffashi, and S. Davoodi, *J. Appl. Polym. Sci.*, **133**, DOI: 10.1002/app.43104 (2016).
23. X. Zhang, E. Koranteng, Z. Wu, and Q. Wu, *J. Appl. Polym. Sci.*, **133**, DOI: 10.1002/app.42983 (2016).
24. W. S. Chow, *Express Polym. Lett.*, **6**, 503 (2012).
25. S. C. Tjonga, S.-A. Xua, R. K.-Y. Lia, and Y.-W. Maic, *Compos. Sci. Technol.*, **62**, 2017 (2002).
26. Y. Y. Leu, Z. A. Mohd Ishak, and W. S. Chow, *J. Appl. Polym. Sci.*, **124**, 1200 (2012).
27. L. Yin, J. Yin, D. Shi, and S. Luan, *Eur. Polym. J.*, **45**, 1554 (2009).
28. J. Jiang, L. Su, K. Zhang, and G. Wu, *J. Appl. Polym. Sci.*, **128**, 3993 (2012).
29. G. Radonjič and I. Šmit, *Polym. Sci. Pol. Phys.*, **39**, 566 (2001).
30. H. Pang, L. Xu, D.-X. Yan, and Z.-M. Li, *Prog. Polym. Sci.*, **39**, 1908 (2014).
31. M. H. Al-Saleh and U. Sundararaj, *Carbon*, **47**, 1738 (2009).
32. N. C. Das, D. Khastgir, T. K. Chaki, and A. Chakraborty, *Compos. Pt. A-Appl. Sci. Manuf.*, **31**, 1069 (2000).